Geology, Geophysics & Environment 2024, vol. 50 (2): 145–154

The effects of component rotation on H/V spectra: a comparison of rotational and translational data

Dariusz Nawrocki[1], Maciej Mendecki[2], Lesław Teper[3]

[1] *University of Silesia in Katowice, Faculty of Natural Sciences, Sosnowiec, Poland, e-mail: dariusz.nawrocki@us.edu.pl (corresponding author), ORCID ID: 0000-0002-3230-1209*
[2] *University of Silesia in Katowice, Faculty of Natural Sciences, Sosnowiec, Poland, e-mail: maciej.mendecki@us.edu.pl, ORCID ID: 0000-0003-0952-3302*
[3] *University of Silesia in Katowice, Faculty of Natural Sciences, Sosnowiec, Poland, e-mail: leslaw.teper@us.edu.pl, ORCID ID: 0000-0002-5065-5676*

Received: 17 October 2023; accepted: 18 April 2024; first published online: 20 May 2024

Abstract: The presented investigation focused on site effect estimations, specifically resonance frequency and amplification. These estimations were carried out for both rotational and translational signals, using waveforms from mining-induced seismic events. Site effect parameters were calculated using the horizontal-to-vertical spectral ratio (HVSR) technique, which is commonly applied to translational records by comparing the spectral ratio between horizontal and vertical components. In this study, we also applied the horizontal-to-vertical (H/V) ratio to rotational records. However, due to the different orientations of motion propagation, we introduced the spectral H/V ratio for rotational motion as the torsion-to-rocking spectral ratio (TRSR). Furthermore, we analyzed these signals according to two approaches. First, we estimated the site effect parameters for directly registered signals, and secondly, we considered rotated components by varying the angle from 0° to 180° in 5-degree increments. Generally, the H/V curves indicated two peaks for translational motions and four peaks for rotational motions. The averaged H/V spectra and spectra obtained for different angles of component rotation showed insignificant fluctuation in amplification values for both rotational and translational motions. However, when comparing each component's spectrum for all angles, we observed changes in the site effect parameter values for both motion types. Radar plots depicting amplification values versus rotation angles for separated components revealed characteristic fluctuations, suggesting local anisotropy. Moreover, when comparing the radar plots between rotational and translational results, it was evident that rotational resonance frequencies shifted to higher frequency values, potentially indicating shallower geological layers as their source.

Keywords: HVSR, time history rotation, rotational motion, site effect, induced seismicity

INTRODUCTION

The estimation of site effect parameters using the horizontal-to-vertical spectral ratio method (HVSR), as described by Nakamura (1989, 2019), is widely recognized in seismological surveys and practice. The amplification spectrum is determined by dividing the horizontal-to-vertical Fourier spectrum of the P-S wave phase or S-wave phase (in the case of analyzing seismic event signals) or signal noise (e.g., Stanko et al. 2017, Zhu et al. 2019, Stanko & Markušić 2020). Peaks observed on the amplification spectrum define the resonance frequency and amplification value. The input data for HVSR estimation can stem from natural seismicity (e.g., Rong et al. 2017, Stanko et al. 2020,) as well as mining-induced seismicity (e.g., Olszewska & Lasocki 2004, Olszewska & Mutke 2018). However, in some cases, determining the main site effect parameters of the spectrum can be challenging due to the presence

https://doi.org/10.7494/geol.2024.50.2.145 ISSN 2299-8004 | e-ISSN 2353-0790 | Wydawnictwa AGH

of multiple amplification peaks on the signal (e.g., Zhu et al. 2019). On the other hand, some research has shown (e.g., Rong et al. 2017) that the derived amplification values may be underestimated compared to standard spectral ratios and can also depend on the orientation of the sensor (Rupakhety & Sigbjörnsson 2013, Pinzón et al. 2019). Following studies presented by Zembaty (2006), a rotational movement was categorized as rocking (around the horizontal axis) and torsion (around the vertical axis). Until recently, the HVSR method was primarily used for determining translational site effect parameters. In light of studies presented by Nawrocki et al. (2021), the concept of the method can be applied to estimate site effect parameters from recordings of rotational motion. Therefore, the HVSR method adapted for rotational motion was described as the torsion-to-rocking spectral ratio (TRSR). Despite TRSR and HVSR addressing different types of motion, the key challenge of reliably determining the main peak remains. Considering the impact of the rotation time history on the amplification spectrum, the following questions arise: Does the rotation of the time history alter the resonance frequency value? Does it induce fluctuations in both site effect parameters? Do rotation procedures yield similar observations for TRSR and HVSR? The presented paper aims to analyze and compare the results of estimating the H/V spectrum for translational and rotational motion after rotating the time history by angles ranging from 0° to 180°. This investigation was conducted at a single seismic station located in the Upper Silesian Coal Basin, where seismic data resulting from mining-induced seismicity were recorded.

DATA AND SITE CHARACTERISTICS

Seismological observations were conducted at a single station known as IMI, located in the Upper Silesian Coal Basin, Poland (Zembaty et al. 2017, Nawrocki et al. 2022) (Fig. 1A).

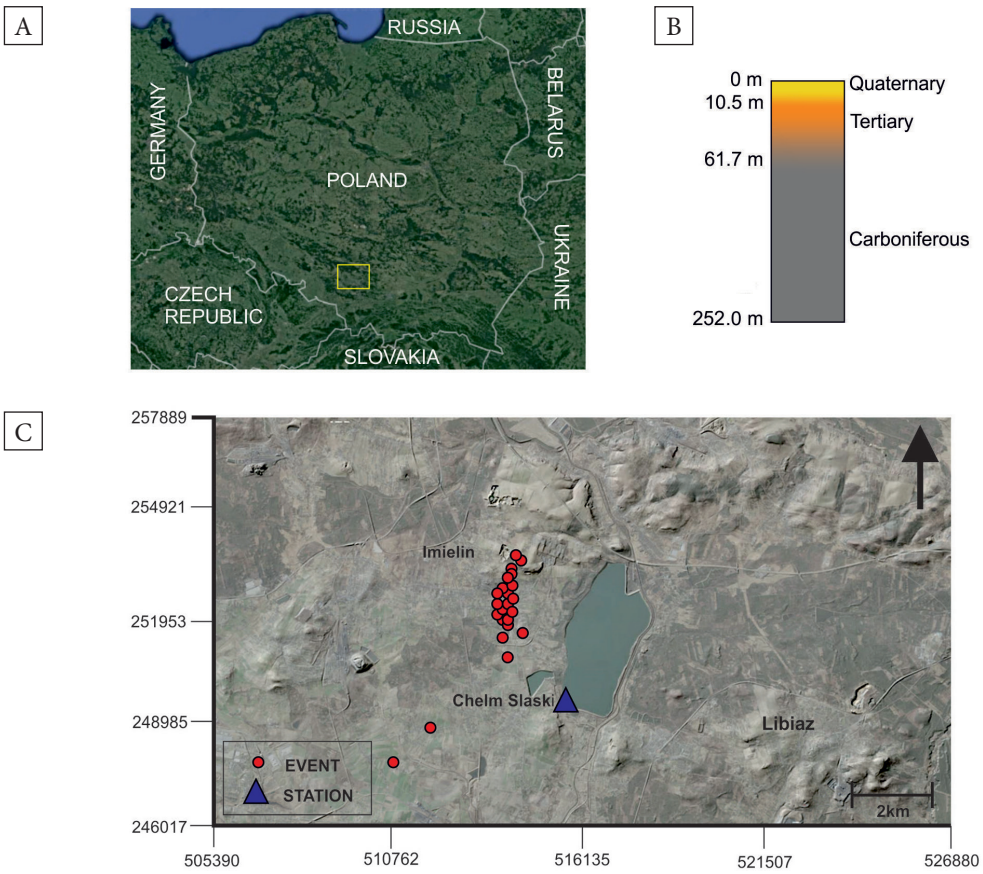

Fig. 1. *Study area information: A) location on the territory of Poland; B) generalized geological profile of the IMI site; C) detailed map of registered seismic events*

Both translational and rotational signals were simultaneously recorded using two independent sensors: a rotational seismometer, R-1 (e.g., Lin et al. 2009, Liu et al. 2009), and a translational accelerometer, EA-120. Both sensors were connected to the DR-4000 data recorder, manufactured by Eentec. The measurement setup was installed at a shallow depth of 1.2 m. The recorded temperature remained stable and below 18°C, eliminating potential issues with the reliability of the rotational sensor (Bernauer et al. 2012). From a geological perspective, the site was characterized by a shallow layer of Quaternary sediments (including sands, pebbles, muds, and alluvia) resting above Triassic sandstones (Buła & Kotas 1994, Jureczka et al. 1995). Beneath these layers, the rigid basement was formed by Carboniferous coal-bearing formations, composed of sandstones, mudstones, and siltstones interbedded with hard coal seams (Sagan et al. 1996, Mendecki et al. 2020, Teper 2000) (Fig. 1B). The estimated average shear wave velocity up to a depth of 30 m reached 408 m/s (Mutke et al. 2020). The seismic catalog comprised 60 registered events, with local magnitudes ranging from 1.7 to 2.7. The estimated epicentral distances varied from 0.75 km to 5.52 km (Fig. 1C), which in connection to the range of the local magnitudes caused high resolution of the recorded seismic signals (Fig. 2). A collection of all recorded seismograms used in the analysis was attached to the article as a supplementary file in online version.

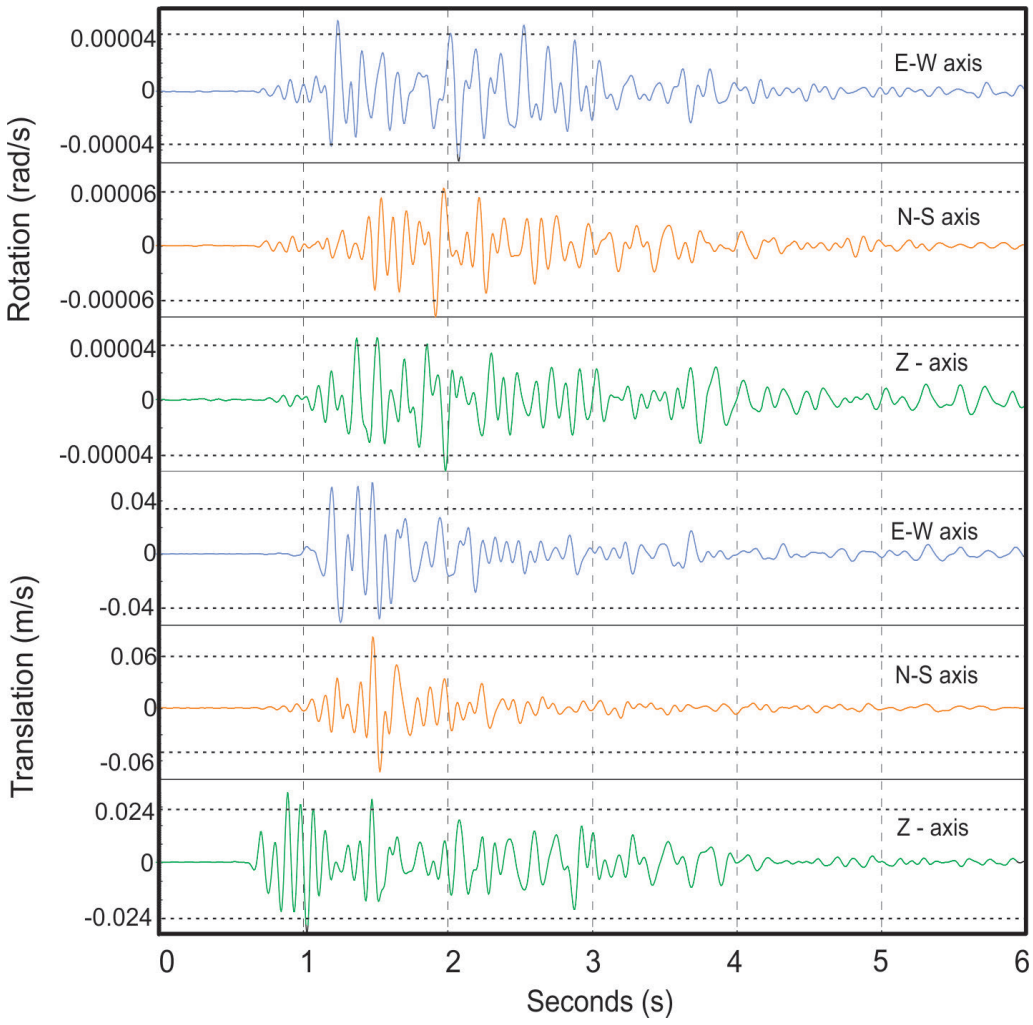

Fig. 2. *Seismogram of the seismic event registered at the IMI station on February 8, 2016, the local magnitude reached 1.93, and the epicentral distance was equal to 0.9 km*

METHODS

Analysis of the registered seismic data was performed for both types of seismic signals (i.e. rotations and translations) in the same way. Firstly, the signal rotation by an angle was performed assuming 5-degree step in the range from 0° to 180° (Fig. 3). The procedure of axes rotation to obtain the rotated amplitude response time histories can be expressed as the following matrix formula:

$$\begin{bmatrix} X_R \\ Y_R \end{bmatrix} = \begin{bmatrix} \cos(\theta) & \sin(\theta) \\ -\sin(\theta) & \cos(\theta) \end{bmatrix} \cdot \begin{bmatrix} X_D \\ Y_D \end{bmatrix} \quad (1)$$

where X_D and Y_D are the direct registered horizontal signals along the E-W and N-S axes, respectively, θ is an angle of axis rotation, and X_R and Y_R determine rotated signals.

The next step involves estimating site effect parameters, namely resonance frequency and amplification value, for each angle of signal rotation. To achieve this, we conducted H/V analysis for the S-wave phase of both signal types (Nakamura 1989, 2019). The expected resonance frequency was anticipated to be lower than 2 Hz, corresponding to the resonance of the Quaternary and Triassic deposits at this site (see Nawrocki et al. 2022). Therefore, following the SESAME criteria (SESAME 2004), the signals were windowed fifty times, each with a duration of approximately four seconds, from the S-wave arrival, which allowed us to mark off the signal part, including multiple reflections of SH waves and therefore a fulfilled statement of the Nakamura approach (Nakamura 1989, 2019).

Subsequently, they were transformed using the fast Fourier transform (FFT) and smoothed using the Konno–Ohmachi logarithmic window function (Konno & Ohmachi 1998). The resulting signals were then processed further. The translational amplification spectrum was derived using the following equation (Zhu et al. 2020):

$$\begin{aligned} &\log_{10} HVSR_{AV}(f) = \\ &= 0.5\left[\log_{10}\left(S_{T_x}(f)\right) + \log_{10}\left(S_{T_y}(f)\right)\right] \\ &- \log_{10}\left(S_{T_z}(f)\right) \end{aligned} \quad (2)$$

where the S determines the result of using Fourier amplitude spectrum for the event signal, and T_x, T_y, and T_z denotes the horizontal and vertical components of the record.

H/V spectral ratio of the rotational motion, called TRSR, can be estimated as the ratio of torsional and rocking components (Sbaa et al. 2017, Ringler et al. 2018, Nawrocki et al. 2021) and described as the following equation:

$$\begin{aligned} &\log_{10} TRSR_{AV}(f) = \log_{10}\left(S_{R_z}(f)\right) \\ &- 0.5\left[\log_{10}\left(S_{R_x}(f)\right) + \log_{10}\left(S_{R_y}(f)\right)\right] \end{aligned} \quad (3)$$

where the S determines the result of using Fourier amplitude spectrum for the event signal, and R_x, R_y, and R_z denotes the rocking and torsion components of the record.

In the end, results from the Equations (2) and (3), for each of the angles of rotation were averaged, which allowed us to calculate the resultant spectrum curve. Since the sensors recorded the signals simultaneously, we were able to extract identical parts of the signals from both rotational and translational records.

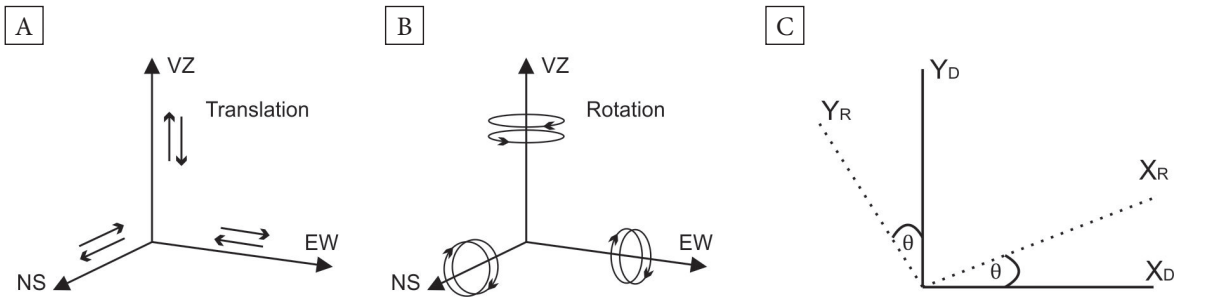

Fig. 3. *Motion directions in translation (A) and rotation (B), and rotation matrix sketch (C)*

RESULTS

The H/V curve of directly registered translational signals revealed two prominent amplification peaks at 1.60 Hz and 2.20 Hz. In contrast, the rotational amplification spectrum exhibited three primary peaks at 1.80 Hz, 3.60 Hz, and 4.60 Hz. However, it has been pointed out by some researchers (e.g., Zhu et al. 2020) that H/V estimation using Fourier amplitude spectrum can yield multiple amplification peaks, making it challenging to determine the true resonance frequency. A suggested solution is to estimate H/V using response spectrum acceleration, which is expected to identify the true peak of the resonance frequency. Therefore, taking into account other research conducted on the same database (see Nawrocki et al. 2022), the general maximum for translational motion was found at 1.60 Hz, while for rotational motion, it was observed at 1.80 Hz and 4.60 Hz. Consequently, further analysis was conducted for the main resonance frequencies mentioned above, which met the SEISAME criteria for general amplification peaks. Rotation of the time history introduced fluctuations in the amplification values. The angles of rotation that resulted in maximum and minimum amplification values are listed in Table 1. In the case of H/V for translational motion components, the difference in angles between the maximum and minimum amplification values ranged from 20° to 30°, while for the averaged H/V, it reached 45°. However, concerning the first peak of rotational H/V, the angle difference for the respective EW and NS components was 90° and 10°, while for averaged H/V, it was 5°. Regarding the second rotational amplification peak, the angle difference for averaged H/V reached 45°, while for the EW and NS components, it was 90°.

Rotation by the angle of the time history of the signal caused changes in the shape of the origin amplification spectrum. In the case of the rotational motion, the rotation of the time history mainly caused changes with the amplification value (Fig. 4A–C).

In the case of translational motion, in addition to fluctuations in amplification values, observable changes in resonant frequencies were noted (see Fig. 4D–F).

Radar plots of the averaged translational motion amplification spectrum (see Fig. 5A) displayed an ellipsoidal structure characterized by a general peak maximum and a medium level of the rest values fluctuation. Similar ellipsoidal structures were observed for the rotational averaged H/V as well. However, the NS and EW components (see Fig. 5B, C) exhibited a distinct trend of higher and lower amplification values. A similar orientation of the NS and EW components was observed for the second amplification maximum of the rotational motion (see Fig. 5D–F). Nevertheless, the components of the first amplification peaks displayed an ellipsoidal structure.

Table 1
Comparison of the minimum, maximum and directly measured amplification value due to rotation of the time history by an angle

Type of motion	Direction	Peak	Frequency range [Hz]	Directly measured		Minimum values		Maximum values	
				amplification	angle	amplification	angle	amplification	angle
Translation	NS	1	1.5–2.0	7.10	0	3.88	130	9.18	110
	EW	1	1.5–2.0	6.70	0	3.99	40	10.83	10
	AV	1	1.5–2.0	6.80	0	5.15	55	12.00	10
Rotation	NS	1	1.0–1.5	3.70	0	2.00	105	3.51	10
		4	4.0–4.7	1.37	0	1.04	135	2.25	45
	EW	1	1.0–1.5	3.10	0	2.00	105	3.62	115
		4	4.0–4.7	1.37	0	1.05	50	2.27	140
	AV	1	1.0–1.5	2.50	0	1.99	105	3.12	110
		4	4.0–4.7	1.32	0	1.31	160	1.37	115

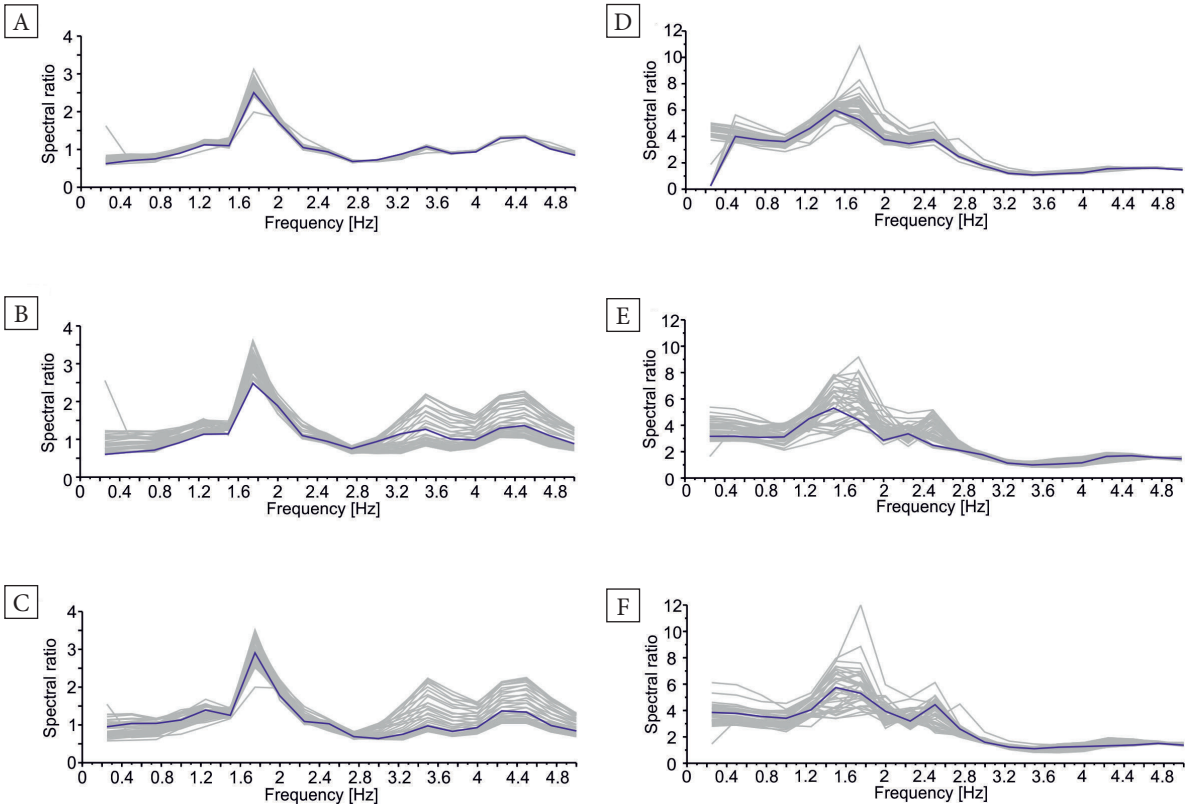

Fig. 4. *H/V curves of directed registered signals (blue line) and rotated (grey lines): A) average TRSR; B) EW-dir TRSR; C) NS-dir TRSR; D) average HVSR; E) EW-dir HVSR; F) NS-dir HVSR*

DISCUSSION

Considering the results of the data analysis presented in Table 1, rotating the time history by an angle led to both increases and decreases in amplification values when compared to the estimated H/V for directly recorded signals. It is worth noting that, based on the results, the angles that produced maximum and minimum values for the first peak of rotational motion were different from those for translational motion. The literature has previously noted the directionality of translational H/V (Rupakhety & Sigbjörnsson 2013, Pinzón et al. 2019), attributing it to the presence of local anisotropy in geological structures such as fractures, faults, and the occurrence of heterogeneous structures, which results in fluctuations in amplification values. Therefore, considering the similar resonant frequency values between the first peak of rotational and translational H/V, suggesting a similar depth of the resonant layer, it can be inferred that rotational H/V is influenced by a different orientation of potential geological anisotropy compared to translational H/V. However, when examining the radar plots (see Fig. 5), it becomes apparent that rotational amplification creates an ellipsoidal structure without a specific orientation of minimum and maximum values. This is in contrast to the translational H/V radar plots. The second rotational amplification peak was observed at 4.60 Hz, which, assuming that the resonance frequency for rotations is similar to that for translations, can be approximated using the formula:

$$F_R = \frac{V_s}{4H} \tag{4}$$

where V_S is the shear velocity of the geological layer, H and F_R mean, respectively, thickness and resonance frequency, leading to the conclusion that the geological layer of the rotational resonance occurred shallower than in the case for translation motions. Thus, comparing the angles associated with maximum and minimum values between translations and rotations may appear unwarranted.

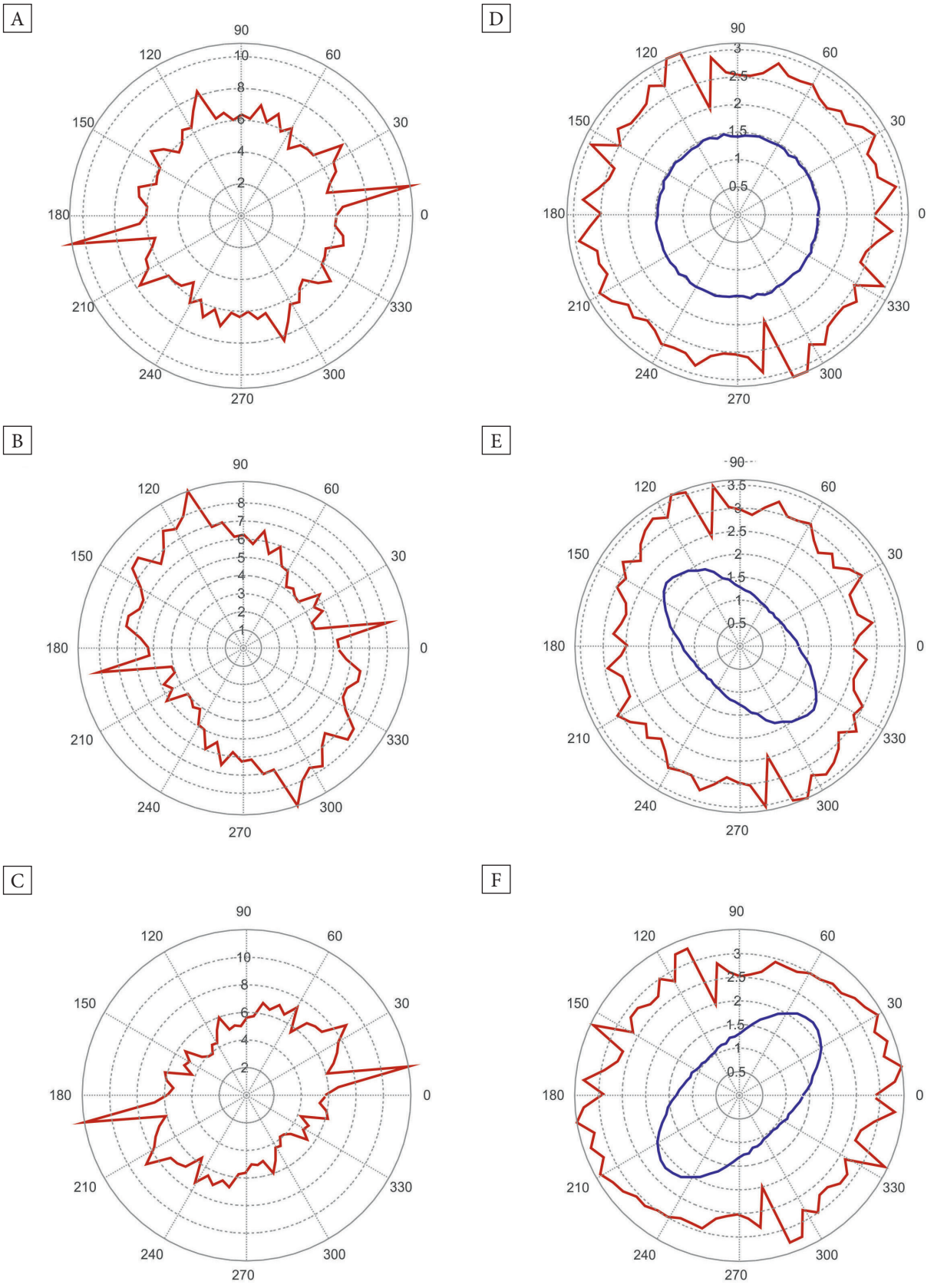

Fig. 5. *Radar plots of H/V curves for rotated data: A) average HVSR; B) EW- dir HVSR; C) NS-dir HVSR; D) average TRSR; E) EW-dir TRSR; F) NS-dir TRSR*

However, considering the results from the radar plots (see Fig. 4), the orientation of the structure between the respective horizontal components of rotational and translational motion displayed strong similarities. This suggests the potential conclusion that the resonant layer, in some cases, may produce varying values for the site effect parameters of rotational and translational motion.

Taking into account the findings presented by Nawrocki et al. (2022), it was suggested that the reason for the different resonance frequency values in rotational and translational motion was linked to the presence of rigid fractured structures (see Fig. 6). The motivation for this explanation was found in studies that investigated the mechanism of rotational source and attributed its occurrence to friction processes or defects within the medium (Kozák 2006, Teisseyre & Kozák 2006). While the possibility of fractures at the site could not be ruled out, based on the resonance frequency of the first rotational peak, it appears that the resonant layer is predominantly compacted (Nawrocki et al. 2022). However, the presented model did not sufficiently explain why higher resonance frequency values in rotational motion correspond to lower values in translational motion (see Fig. 6). Therefore, assuming that the directionality observed in translational H/V results from the presence of local anisotropy, and considering that the directionality orientation of translational motion aligns with the directionality orientation of rotational motion at higher resonance frequency values, it leads to the conclusion that site effect parameters for rotation and translation motion may differ even within the same geological structure.

Another aspect concerns the resonance frequency value of the primary H/V peak. In the case of translational motion (see Fig. 4), fluctuations in resonance frequency were observed. Considering the equation provided above (Equation (4)), changes in resonance frequency values are linked to the depth at which the resonance layer occurs. The fluctuation between directly measured data and rotated time histories reached 0.4 Hz. Considering the measured value of the averaged shear wave velocity up to 30 m, which reached 408 m/s (Mutke et al. 2020), the depth of the resonance layer changed within the range of 62–57 m.

Conversely, a different situation was observed for both amplification peaks in rotational H/V, where the resonance frequency value remained constant. Despite the rotation of the time history, it appears that the resonant layer of rotational motion did not exhibit changes in depth levels for each of the defined amplification peaks.

The last aspect concerned on the Rayleigh wave is an impact on the estimation of the S-wave phase H/V spectrum (Nakamura 2019). The minimum distance of the Rayleigh waves generation is given by the formula (Okamoto 1984):

$$s_s = \frac{V_R}{\sqrt{\beta^2 - V_R^{\,2}}} d \tag{5}$$

where V_R is the Rayleigh wave velocity equalled 0.9β, β is the shear wave velocity, and d denotes the depth of the event source.

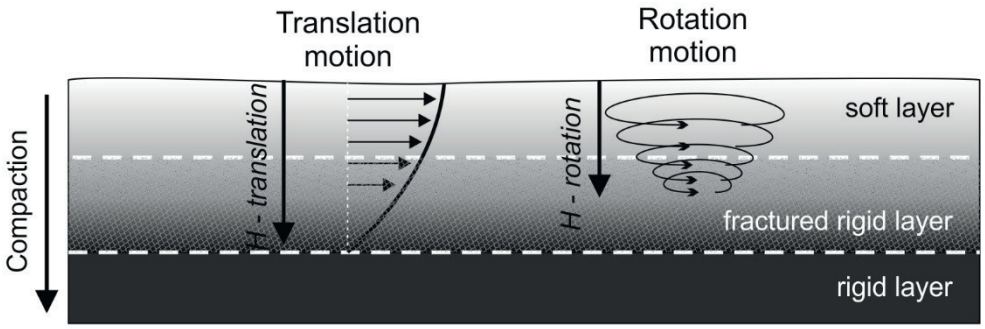

Fig. 6. *Models of translation and rotation resonance effects with amplified horizontal amplitudes in near-surface and different depth ranges (after Nawrocki et al. 2022)*

The event depths ranged 1.0–1.2 km, while the shear wave velocity of the surface layer was 2080 m/s. Consequently, the minimal distance of Rayleigh wave generation ranged 2.0–2.4 km. The dataset taken into the analysis excludes the presence of the Rayleigh waves on the 54 registered signals, which was motivated by the meagre distance between the event source and the station, up to 2.0 km. The rest of the events were characterized by the epicentral distance, which was 4.0–5.5 km, and in consequence, the signal of the Rayleigh wave occurred. Nevertheless, their influence on the estimated H/V spectrum was negligible.

CONCLUSIONS

The presented study showed an estimation of the site effect parameters for directly measured and also for rotated signals of rotational and translational motion. The H/V spectrum, derived for each case of rotated signals, finally presented the fluctuation of the site effect parameter values, which suggested the occurrence of local anisotropy. The H/V spectrum of horizontal components, estimated for rotated time history, produced a characteristic ellipsoidal structure, which may indicate the local anisotropy orientation. The ellipsoidal structure orientation was comparable to the general amplification peak of the translations (1.60 Hz) and a third peak of the rotations (4.60 Hz). Considering the dependence of the resonance frequency value on the shear velocity and thickness, rotational amplification should be produced by shallower geological layers than in the case of translations. That subjection was fulfilled in the case of the comparisons between the first translational and rotational amplification peaks. However spatial orientation of the amplification structures produced incomparable results. Therefore, the possibility of the dependence of the site effect values for the same geological structure on the analyzed type of motion cannot be rejected.

The authors would like to thank Professor Grzegorz Mutke from the Central Mining Institute, Poland, for sharing the registered seismological data, including rotational and translational data from the seismic station.

REFERENCES

Bernauer F., Wassermann J. & Igel H., 2012. Rotational sensors – a comparison of differentsensor types. *Journal of Seismology*, 16(4), 595–602. https://doi.org/10.1007/s10950-012-9286-7.

Buła Z. & Kotas A. (eds.), 1994. *Atlas geologiczny Górnośląskiego Zagłębia Węglowego. Część III: Mapy geologiczno-strukturalne* [*Geological atlas of the Upper Silesian Coal Basin. Part III: Structural-geological maps: 1:100 000*]. Państwowy Instytut Geologiczny, Warszawa.

Jureczka J., Aust J., Buła Z., Dopita M. & Zdanowski A., 1995. *Geological map of the Upper Silesian Coal Basin (Carboniferous subcrop) 1:200 000*. Państwowy Instytut Geologiczny, Warszawa.

Konno K. & Ohmachi T., 1998. Ground-motion characteristics estimated from spectral ratio between horizontal and vertical components of microtremor. *Bulletin of the Seismological Society of America*, 88(1), 228–241. https://doi.org/10.1785/BSSA0880010228.

Kozák J.T., 2006. Development of earthquake rotational effect study. [in:] Teisseyre R., Majewski E. & Takeo M. (eds.), *Earthquake Source Asymmetry, Structural Media and Rotation Effects*, Springer, Berlin, Heidelberg, 3–10. https://doi.org/10.1007/3-540-31337-0_1.

Lin C.-J., Liu C.-C. & Lee W.H.K., 2009. Recording rotational and translational ground motions of two TAIGER explosions in northeastern Taiwan on 4 March 2008. *Bulletin of the Seismological Society of America*, 99(2B), 1237–1250. https://doi.org/10.1785/0120080176.

Liu C.-C., Huang B.-S., Lee W.H.K. & Lin C.-J., 2009. Observing rotational and translational ground motions at the HGSD station in Taiwan from 2007 to 2008. *Bulletin of the Seismological Society of America*, 99(2B), 1228–1236. https://doi.org/10.1785/0120080156.

Mendecki M.J., Szczygieł J., Lizurek G. & Teper L., 2020. Mining-triggered seismicity governed by a fold hinge zone: The Upper Silesian Coal Basin, Poland. *Engineering Geology*, 274, 105728. https://doi.org/10.1016/j.enggeo.2020.105728.

Mutke G., Lurka A. & Zembaty Z., 2020. Prediction of rotational ground motion for mining-induced seismicity – Case study from Upper Silesian Coal Basin, Poland. *Engineering Geology*, 276, 105767. https://doi.org/10.1016/j.enggeo.2020.105767.

Nakamura Y., 1989. A method for dynamic characteristics estimation of subsurface using microtremor on the ground surface. *Quarterly Report of Railway Technical Research Institute*, 30(1), 25–33.

Nakamura Y., 2019. What is the Nakamura method? *Seismological Research Letters*, 90(4), 1437–1443. https://doi.org/10.1785/0220180376.

Nawrocki D., Mendecki M. & Teper L., 2021. Rotational-translational scaling relations from induced seismic events – comparison before and after amplification correction. *Exploration Geophysics, Remote Sensing and Environment*, 28(2), 18–28. https://doi.org/10.26345/egrse-018-21-202.

Nawrocki D., Mendecki M. & Teper L., 2022. Estimation of site resonance frequency using HVSR method for rotational and translational signals: result comparison from Fourier and response spectrum methods. [in:] Arion C., Scupin A., Ţigănescu A. (eds.), *Proceedings of the Third*

European Conference on Earthquake Engineering and Seismology – 3ECEES: September 4 – September 9 2022, Bucharest, Romania, Conspress, Bucureşti, 4539–4546.

Okamoto S., 1984. *Introduction to Earthquake Engineering*. 2nd ed. University of Tokyo Press, Tokyo.

Olszewska S., 2004. Application of the horizontal to vertical spectral ratio technique for estimating the site characteristics of ground motion caused by mining induced events. *Acta Geophysica Polonica*, 52(3), 301–318.

Olszewska D. & Mutke G., 2018. *A study of site effect using surface-downhole seismic data in a mining area* [paper presentation]. 16th European Conference on Earthquake Engineering, 18–21 June 2018, Thessaloniki, Greece. https://episodesplatform.eu/eprints/2123/1/Olszewska_Mutke_1ECEE_fin2_20180305.pdf.

Pinzón L.A., Pujades L.G., Macau A., Carreño E. & Alcalde J.M., 2019. Seismic site classification from the horizontal-to-vertical response spectral ratios: Use of the Spanish strong-motion database. *Geosciences*, 9(7), 294. https://doi.org/10.3390/geosciences9070294.

Ringler A., Anthony R., Holland A., Wilson D. & Lin C.J., 2018. Observations of rotational motions from local earthquakes using two temporary portable sensors in Waynoka, Oklahoma. *Bulletin of the Seismological Society of America*, 108(6), 3562–3575. https://doi.org/10.1785/0120170347.

Rong M., Fu L.-Y., Wang Z., Li X., Carpenter N.S., Woolery E.W. & Lyu Y., 2017. On the amplitude discrepancy of HVSR and site amplification from strong-motion observations. *Bulletin of the Seismological Society of America*, 107(6), 2873–2884. https://doi.org/10.1785/0120170118.

Rupakhety R. & Sigbjörnsson R., 2013. Rotation-invariant measures of earthquake response spectra. *Bulletin of Earthquake Engineering*, 11(6), 1885–1893. https://doi.org/10.1007/s10518-013-9472-1.

Sagan G., Teper L. & Zuberek W.M., 1996. Tectonic analysis of mine tremor mechanisms from the Upper Silesian Coal Basin. *Pure and Applied Geophysics*, 147(2), 217–238. https://doi.org/10.1007/BF00877479.

Sbaa S., Hollender F., Perron V., Imtiaz A., Bard P.-Y., Mariscal A., Cochard A. & Dujardin A., 2017. Analysis of rotation sensor data from the SINAPS@ Kefalonia (Greece) post-seismic experiment – link to surface geology and wavefield characteristics. *Earth, Planets and Space*, 69, 124. https://doi.org/10.1186/s40623-017-0711-6.

SESAME: Site EffectS assessment using AMbient Excitations, 2004. *Guidelines for the implementation of the H/V spectral ratio technique on ambient vibrations: Measurements, processing and interpretation*. SESAME European Research Project, WP12 – Deliverable D23.12, European Commission – Research General Directorate.

Stanko D. & Markušić S., 2020. An empirical relationship between resonance frequency, bedrock depth and VS30 for Croatia based on HVSR forward modelling. *Natural Hazards*, 103(3), 3715–3743. https://doi.org/10.1007/s11069-020-04152-z.

Stanko D., Markušić S., Strelec S. & Gazdek M., 2017. HVSR analysis of seismic site effects and soil-structure resonance in Varaždin city (North Croatia). *Soil Dynamics and Earthquake Engineering*, 92, 666–677. https://doi.org/10.1016/j.soildyn.2016.10.022.

Teper L., 2000. Geometry of fold arrays in the Silesian-Cracovian region of southern Poland. [in:] Cosgrove J.W. & Ameen M.S. (eds.), *Forced Folds and Fractures*, Geological Society Special Publication, 169, The Geological Society, London, 167–179. https://doi.org/10.1144/gsl.sp.2000.169.01.12.

Zembaty Z., 2006. Deriving seismic surface rotations for engineering purposes. [in:] Teisseyre R., Takeo M. & Majewski E. (eds.), *Earthquake Source Asymmetry, Structural Media and Rotation Effects*, Springer, Berlin, Heidelberg, 549–568. https://doi.org/10.1007/3-540-31337-0_38.

Zembaty Z., Mutke G., Nawrocki D. & Bobra P., 2017. Rotational ground-motion records from induced seismic events. *Seismological Research Letters*, 88(1), 13–22. https://doi.org/10.1785/0220160131.

Zhu C., Cotton F. & Pilz M., 2020. Detecting site resonant frequency using HVSR: Fourier versus response spectrum and the first versus the highest peak frequency. *Bulletin of the Seismological Society of America*, 110(2), 427–440. https://doi.org/10.1785/0120190186.

Supplementary data associated with this article (all of the registered rotational and translational seismograms on which the presented analysis was carried out) can be found, in the online version, at:
https://doi.org/10.7494/geol.2024.50.2.145